Band dispersions of Ag(111) monolayers on various substrates

A. P. Shapiro,* T. C. Hsieh,† A. L. Wachs,‡ T. Miller, and T.-C. Chiang
Department of Physics and Materials Research Laboratory, University of Illinois at Urbana-Champaign, 1110 West Green Street, Urbana, Illinois 61801
(Received 10 March 1988; revised manuscript received 9 May 1988)

This paper describes angle-resolved photoemission and high-energy electron diffraction studies of the growth and electronic properties of Ag monolayers prepared on Ni(111), Ni(001), Cu(111), Cu(001), Au(111), and Si(111)-(7×7). In all six systems, the Ag overlayer structure is very close to the hexagonal close-packed Ag(111) structure. Thus the effect of the substrate can be studied without the complication of major structural changes in the overlayer. The two-dimensional band dispersions for the Ag valence states have been determined along high-symmetry directions for these systems except Ag-Si(111). The Ag overlayers on Cu(111), Ni(001), and Ni(111) are incommensurate with the substrate structure, and the overlayer band dispersions are very similar despite the large differences in the electronic and atomic structures of the substrates. Ag on Cu(001) forms a $c(10\times2)$ overlayer, and the photoemission results are somewhat different. Ag on Au(111) forms a lattice-matched epitaxial overlayer, and its band dispersions have a very different appearance. These similarities and differences are explained in terms of the degree of commensuration of the substrate-overlayer interaction as a perturbation on the overlayer properties. The growth of Ag on Si(111)-(7×7) is not as well ordered as in the other systems. A severe broadening of the overlayer photoemission features is observed, preventing the determination of the band dispersions. Momentum broadening as well as random crystal potential variation within the overlayer are likely to be the cause of the broadening.

I. INTRODUCTION

In recent years, there has been considerable interest in the studies of thin films. With modern materials preparation techniques, it is now possible to grow smooth monolayers (a single atomic layer) on a variety of substrates. The reduced dimensionality in monolayer films relative to the bulk materials can have dramatic effects on the electronic properties. In addition, the overlayer-substrate interaction can play an important role in modifying the overlayer properties. These are fundamental issues in regard to a detailed understanding of the physics of thin films.

Although a number of experimental and theoretical studies have been performed on thin-film systems,[1–16] little is known about the relationship between the overlayer electronic properties and such physical factors as the substrate material, the substrate surface configuration, and overlayer atomic configuration and order. This is a challenging problem because different competing effects have to be distinguished and identified. The majority of theoretical studies to date have examined unsupported monolayers and thin films;[17–22] however, production of such structures is not feasible yet. A few recent theoretical calculations for metal overlayers indicated that the two-dimensional band dispersions are modified substantially from those of corresponding unsupported monolayers by the substrate-overlayer interaction, although one earlier calculation indicated otherwise.[7,16]

A number of factors must be considered in the selection of systems comprising a systematic study of the electronic properties of monolayers. A large number of materials intermix or alloy under usual conditions of thin-film preparation. Although intermixing and alloying of materials are topics of great importance, they complicate interpretations of data from studies of the sort described here. In addition, the overlayer material should grow in an ordered layer-by-layer fashion on the chosen substrate. The above "requirements," therefore, greatly restrict the number of possible choices of substrate surfaces and overlayer materials. Silver is an example of an overlayer material which meets or approximately meets the above specifications on a considerable set of substrates.

This paper describes a study of Ag monolayers grown on Ni(111), Ni(001), Cu(111), Cu(001), Au(111), and Si(111)-(7×7). In all six systems, the Ag overlayer structure is very close to the hexagonal close-packed Ag(111) structure, as determined by high-energy electron diffraction (HEED). This greatly simplifies comparisons of the overlayer electronic structures since major changes in the overlayer atomic configurations are avoided. Thus, the main remaining effect should be the overlayer-substrate interaction. There are numerous differences among the six systems. Three epitaxial relationships are observed: incommensurate, commensurate, and lattice matched. Four different substrate materials are utilized, one of which is a semiconductor. Thus, the results can provide a useful data basis for empirical identification of the relevant factors that may affect the overlayer electronic structure. From the photoemission data, the two-dimensional band dispersion curves are determined, which show interesting variations for different substrates. These results will be presented and discussed below.

II. EXPERIMENTAL DETAILS

The five metal substrates, Ni(111), Ni(001), Cu(111), Cu(001), and Ag(111) [used as a base for epitaxial growth of the Au(111) substrate], were cut from pure single-crystal ingots using electrical discharge machining, and were aligned with Laue x-ray backscattering. Each was then mechanically polished to a mirror finish with alumina grits; the finishing grit size was 0.3 μm. Chemical etching or electropolishing was employed to remove surface damage from the mechanical polishing.[23] The Ag sample was chemically etched in a dilute KCN solution, whereas a hot solution containing sulfuric, phosphoric, nitric, and acetic acids was used to chemically etch the Ni(111) sample. The Ni(001) sample was electropolished in a 55% sulfuric acid solution, while both Cu samples were electropolished using a 59% phosphoric acid solution. The Si(111) sample was cut from a commercially polished wafer and thus required no pretreatment.

The metal samples were cleaned in the photoemission chamber with repeated cycles of 1-keV Ar-ion sputtering and annealing. The annealing temperatures of the Ni samples were 900 °C during the cleaning cycles and 600 °C for the final anneal. The higher annealing temperature caused trace bulk contaminants (mainly sulfur) to diffuse quickly to the surface where they could be sputtered away; these impurities were depleted after a large number of cleaning cycles. The lower-temperature final anneal was found to produce the optimum clean and well-ordered surface. Once prepared, the Ni samples remained clean for about 2 h. The annealing temperatures for the two Cu samples and the Ag sample were 500 and 320 °C, respectively; once prepared, they remained clean for more than 24 h. The treatment of the Si(111) sample involved heating to about 1200 °C for about 10 s to remove the surface oxide layer, resulting in a reconstructed Si(111)-(7×7) surface which remained clean for about 4 h. The sample cleanliness was checked with Auger spectroscopy. The cleanliness of the Ni(111), Cu(111), Ag(111), and Si(111)-(7×7) samples was also verified with observations of the well-known surface states in photoemission.[24–28]

The Au(111) substrate was prepared by growing 60 Å of Au, or 25 monolayers (ML), on the clean Ag(111) base substrate at room temperature. Ag and Au have a very small lattice mismatch (0.2%). Consequently, Au(111) grows epitaxially in a smooth layer-by-layer fashion on Ag(111) as verified by HEED and other previous studies.[29–31] The Au(111) surface also showed an intense surface state feature in the angle-resolved photoemission spectra.[24]

HEED was used to characterize the quality and reconstruction of the substrate surfaces and the epitaxial relationship and growth of the overlayer films. A 10-keV electron beam energy was used. All clean substrates showed a sharp (1×1) pattern except Si(111) which showed a (7×7) pattern. Ag overlayers were grown by evaporation from Ta or W boats at typical rates of 0.05–0.1 Å/s, which were determined by using a water-cooled quartz crystal thickness monitor immediately prior to each overlayer preparation. 1 ML of Ag(111) corresponds to 2.4-Å thickness. Both Ni samples were heated to near 150 °C during deposition, while the other samples were approximately at room temperature. The attained thicknesses were accurate to within about ±15%, which is limited by the stability of the evaporation rate and the absolute calibration of the thickness monitor itself.[32,33]

After Ag deposition, some of the samples were annealed. The optimum annealing temperatures were determined from extensive HEED, photoemission, and Auger studies. Increasing the annealing temperature generally improved the overlayer order as observed with HEED and indicated by the sharpness of photoemission features (such as a surface state). The annealing temperatures used for Ag-Cu(111), Ag-Cu(001), Ag-Ni(111), and Ag-Ni(001) were 200, 200, 300, and 450 °C, respectively; no further improvement in film ordering was observed by going to higher temperatures. For Ag on Si, even a mild annealing ($\sim$100 °C) would cause the Ag to form a $\sqrt{3}$ layer plus three-dimensional islands.[34] For Ag on Au, a mild annealing would cause the Ag and Au to intermix.[35] Therefore, no annealing was performed for these two systems.

The photoemission experiments were performed at the Synchrotron Radiation Center of the University of Wisconsin–Madison in Stoughton, Wisconsin. The photoelectrons were collected and analyzed by a hemispherical analyzer with a full acceptance angle of 3°. The analyzer was mounted on a two-axis goniometer. The geometric relationship between the crystallographic axes of the sample and the analyzer collection direction was experimentally determined *in situ* by a combination of HEED and optical methods using the visible part of the synchrotron radiation to line up the sample surface normal direction. The angular accuracy was better than ±1°. The binding energy of the photoemission spectra to be presented below is referred to the Fermi level of the substrate. The Fermi-level reference was the measured energy at half height of the Fermi edge in the photoemission spectra. Where surface states or *d*-band features interfered with the measurement, as in the case of Ni, the Fermi edge of a polycrystalline gold foil in electrical contact with the sample was used as the reference instead.

III. RESULTS

A. HEED and structure

All of the metal samples have the face-centered-cubic (fcc) crystal structure. Si has the diamond structure; its underlying lattice is also fcc. The lattice constants of Ni, Cu, Ag, Au, and Si are 3.52, 3.61, 4.09, 4.08, and 5.43 Å, respectively. Thus, there is a large lattice mismatch in these overlayer systems except Ag on Au. The atomic configurations of the surface layer of the unreconstructed substrates are illustrated in Figs. 1(a) and 1(b). The (001) surface layer of a fcc crystal has the structure of a square lattice with a fourfold symmetry, and the (111) surface layer has the structure of a hexagonal lattice with a sixfold symmetry. If layer stacking is considered, however, a (111) fcc sample face actually exhibits a threefold symmetry.

The simplest growth configuration is the nearly perfect layer-by-layer epitaxial growth of Ag(111) on Au(111).[29–31,35] The two lattices are closely matched, and the overlayer growth continues the fcc stacking sequence across the interface. Ag(111) grows unstrained on Cu(111), Ni(111), and Si(111); the large lattice mismatch causes the overlayer to ignore the underlying substrate atomic structure resulting in an incommensurate growth; however, the corresponding crystallographic axes of the overlayer and the substrate are mutually parallel (parallel epitaxy).[2,32,36–38]

The Ag overlayer on Ni(001) also exhibits the Ag(111) structure. But due to differences in substrate and overlayer symmetry (fourfold versus sixfold), the overlayer grows in domains with two orthogonal orientations: Ag[$\bar{1}$10] parallel to either Ni[110] or to Ni[$\bar{1}\bar{1}$0].[2,39] With this arrangement, the overlayer and substrate are very close to being commensurate in one direction due to the approximately $\sqrt{3}/2$ ratio between the Ag and Ni lattice constants. The two domain types are equally populated since the associated HEED features are observed to have equal intensities.

Ag forms a $c(10\times2)$ overlayer on Cu(001) for 1 ML coverage. The structure is a slightly strained Ag(111) monolayer compressed and expanded by about 2% in two orthogonal directions; the areal density of Ag atoms is essentially unchanged by the strain.[4–6] Because of the difference in overlayer and substrate symmetry, the overlayer grows in two orthogonal domains, similar to the case of Ag on Ni(001).

For this study, it is important that there is no significant growth beyond the first monolayer. In all of the systems studied, the overlayers grow in a nearly layer-by-layer fashion at low coverages; thus, a nearly complete layer of Ag is formed before growth of the next layer begins. For the Cu(001) data to be presented below, 1 ML of Ag was used so that the $c(10\times2)$ structure became fully developed as verified by HEED. For Ag on Cu(111), Ni(001), Ni(111), and Au(111), large monolayer-thick Ag(111) islands are formed at coverages below 1 ML as verified by HEED and by the observation that the Ag-derived features in the photoemission spectra have a fixed line shape and an intensity linearly proportional to coverage. Beyond 1-ML coverages, extra photoemission features associated with Ag atoms in the second layer appear, and their intensities are proportional to the Ag coverage in excess of 1 ML. To allow for possible small errors in coverage determination, most of the Ag-Cu(111), Ag-Ni(001), Ag-Ni(111), and Ag-Au(111) data are for $\frac{1}{2}$, $\frac{1}{2}$, $\frac{1}{2}$, and $\frac{3}{4}$ ML Ag coverage, respectively. The HEED patterns from these systems showed very sharp Ag(111) hexagonal patterns superimposed on a (1×1) substrate pattern; occasionally, some weak double diffraction spots were also observed.

A coverage of $\frac{3}{4}$ ML was used in the Ag-Si(111) system. At this coverage, the (7×7) reconstruction of the Si substrate surface was suppressed. HEED showed a fuzzy Ag(111) pattern superimposed upon a Si(111)-(1×1) pattern in a parallel-epitaxy configuration; lower Ag coverages produced HEED patterns with inferior qualities. It has been determined that Ag grows on Si(111) in a nearly layer-by-layer fashion,[36,37] but the overlayer is not as well ordered and smooth as compared with the other systems described above. The disorder is probably partially induced by substrate surface corrugation.

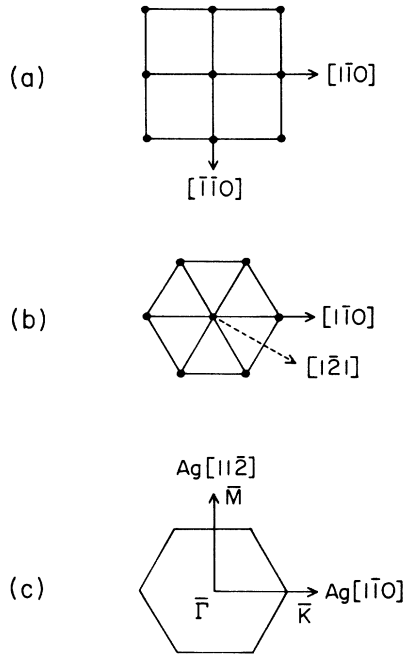

FIG. 1. Configurations of the surface atoms on (a) an unreconstructed (001) face of an fcc crystal and (b) an unreconstructed (111) face of fcc or diamond crystal. The dots represent atoms in the outermost surface layer on each face; several bulk crystallographic directions are indicated. The diagram in (c) shows the two-dimensional Brillouin zone of monolayer Ag(111).

B. Angle-resolved photoemission

The photoemission geometry is indicated in Fig. 2. The sample normal, either [111] or [001], lies along the z axis. All of the substrates were mounted with the [1$\bar{1}$0] direction parallel to the y axes. Photons of energy $h\nu$ are incident in the yz plane at a polar angle θ_I of 60° for the

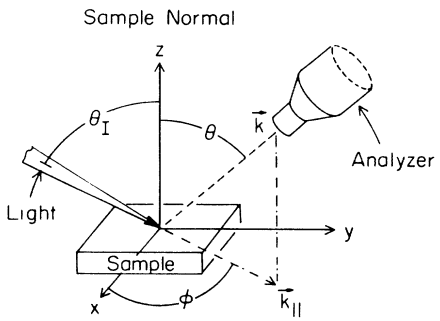

FIG. 2. Photoemission geometry.

metal substrates and 55° for the Si substrate. The light is nearly plane-polarized in the yz plane. The input of the analyzer is at the polar angle θ and azimuthal angle ϕ. When θ and/or ϕ are changed, there is a corresponding change in the component of the photoelectron wave vector in the plane of the sample surface, $\mathbf{k}_{\parallel}$; thus, the two-dimensional band dispersions for the overlayer electronic states can be determined as a function of $\mathbf{k}_{\parallel}$. The two-dimensional Brillouin zone of monolayer Ag(111) is shown in Fig. 1(c). Two types of high-symmetry directions, $\bar{\Gamma}\bar{K}$ and $\bar{\Gamma}\bar{M}$, are shown together with the corresponding crystallographic directions in bulk Ag(111). The magnitudes of $k_{\parallel}$ at the points $\bar{M}$ and $\bar{K}$ are 1.25 and 1.45 Å^{-1}, respectively.

For Ag on Si(111), Au(111), Ni(111), and Cu(111), photoemission spectra were taken with $\mathbf{k}_{\parallel}$ along the substrate $[1\bar{1}0]$ ($\phi=90°$) and $[1\bar{2}1]$ ($\phi=60°$) directions, corresponding to scanning along $\bar{\Gamma}\bar{K}$ and $\bar{\Gamma}\bar{M}$ in the Ag overlayer, respectively. For Ag-Ni(001) and Ag-Cu(001), $\mathbf{k}_{\parallel}$ was chosen to lie along the substrate $[1\bar{1}0]$ ($\phi=90°$) and $[\bar{1}\,\bar{1}0]$ ($\phi=0°$) directions; because of the existence of domains in two orthogonal orientations, both $\bar{\Gamma}\bar{K}$ and $\bar{\Gamma}\bar{M}$ directions were probed simultaneously in each case. Thus the two scans for each (001)-substrate system should produce identical peak positions but not necessarily the same peak intensities.

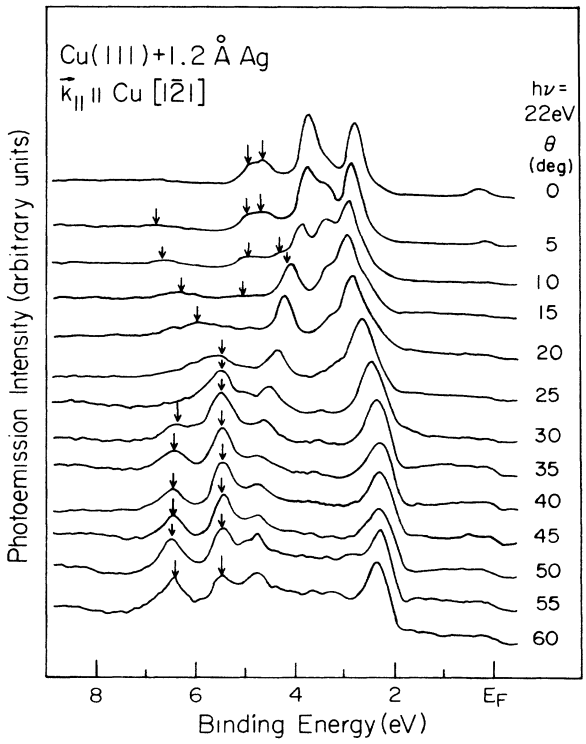

FIG. 3. Angle-resolved photoemission spectra from 1.2 Å ($\frac{1}{2}$ ML) of Ag on Cu(111) taken with a photon energy of 22 eV. The direction of $\mathbf{k}_{\parallel}$ in the scan and the polar emission angles θ are indicated. Features which are due to the presence of the Ag overlayer are marked with arrows. The binding energies are referred to the Fermi level at E_F.

Similar spectra were taken for the bare substrates in each case to aid the identification of the overlayer-derived features. A photon energy of 22 eV was used for most of the measurements. For Ag on Au(111), most of the data were taken with a 32-eV photon energy due to limitations of the monochromator used at that time. Photoemission intensities in spectra taken with different photon energies cannot be compared directly. In all cases, the two-dimensional nature of the overlayer states at the surface Brillouin-zone center was verified by observing that the binding energies of the peaks are not changed for several different photon energies (spectra not shown here).

Figure 3 shows a set of angle-resolved photoemission spectra for $\frac{1}{2}$ ML of Ag on Cu(111) with $\mathbf{k}_{\parallel}$ along the Cu$[1\bar{2}1]$ direction; the polar angle of emission θ is indicated for each spectrum. Figure 4 shows a set of spectra taken under similar conditions but without the Ag overlayer. By comparing the two sets, features derived from the Ag overlayer can be easily identified; these are marked with vertical arrows in Fig. 3. Figure 5 shows the spectra for Ag-Cu(111) with $\mathbf{k}_{\parallel}$ along the Cu$[1\bar{1}0]$ direction. The Ag-derived features are marked as before. To conserve space, the corresponding set of spectra for the bare substrate is not shown here. Likewise, the comparison spectra for the other substrates except Au(111) will not be presented. There is little overlap between the Ag overlayer features and the Ni substrate features, because the Ni and Ag d bands are well separated in energy. The Si substrate sp-band emission is very much weaker than the Ag d-band emission with the photon energy

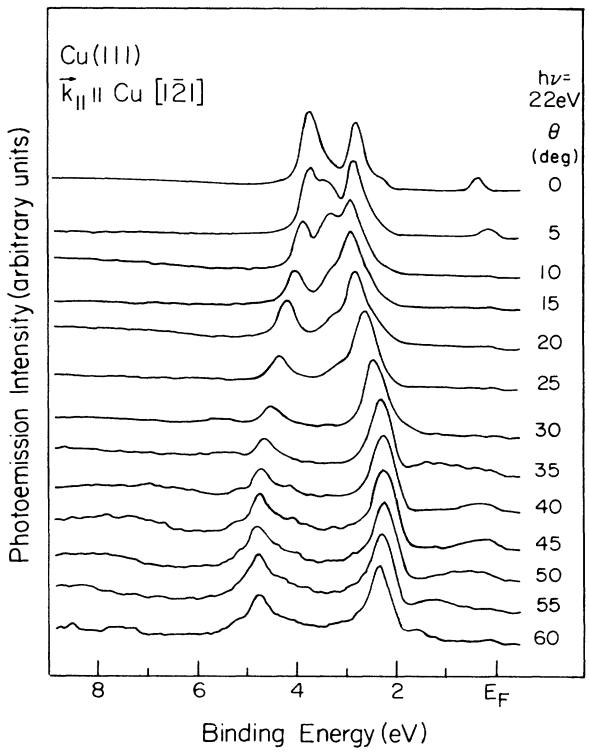

FIG. 4. Same as Fig. 3 except that the sample is clean Cu(111) without the Ag overlayer.

used; therefore, even though they overlap, the Ag band features can still be easily identified.

Figure 6 shows a set of spectra for a $c(10\times2)$ monolayer of Ag on Cu(001) with $\mathbf{k}_{\parallel}$ along the Cu[$\bar{1}\,\bar{1}\,0$] direction; the polar angle of emission for each spectrum is indicated. The Ag-derived features are again marked with vertical arrows. Figure 7 shows another set of spectra taken with $\mathbf{k}_{\parallel}$ along the Cu[$1\bar{1}0$] direction. Similarly, Figs. 8 and 9 show the spectra for Ag on Ni(111) along the two high-symmetry directions as labeled. Figure 10 shows the spectra for Ag on Ni(001) for $\mathbf{k}_{\parallel}$ along the Ni[$\bar{1}\,\bar{1}\,0$] direction; the corresponding set of spectra for $\mathbf{k}_{\parallel}$ along the Ni[$1\bar{1}0$] direction has been published in a previous paper and will not be reproduced here.[2] Some of the overlayer peaks in these spectra are very close, and can be clearly identified only in the original large plots. The assignment of the peak positions in some cases was aided by interpolation and extrapolation from additional spectra (not shown here) taken with slightly different angles and different photon energies.

The data for $\frac{3}{4}$ ML of Ag on Au(111) are shown in Figs. 11 and 12 for the two high-symmetry directions. The comparison spectra taken under similar conditions but without the overlayer are shown in Figs. 13 and 14. Clearly, there is substantial overlap between the Ag and Au spectral features. To aid identification of the overlayer-related features, difference spectra were generated by subtracting the spectra for the bare substrate from the corresponding spectra for the same substrate covered with Ag; the results are shown in Figs. 15 and

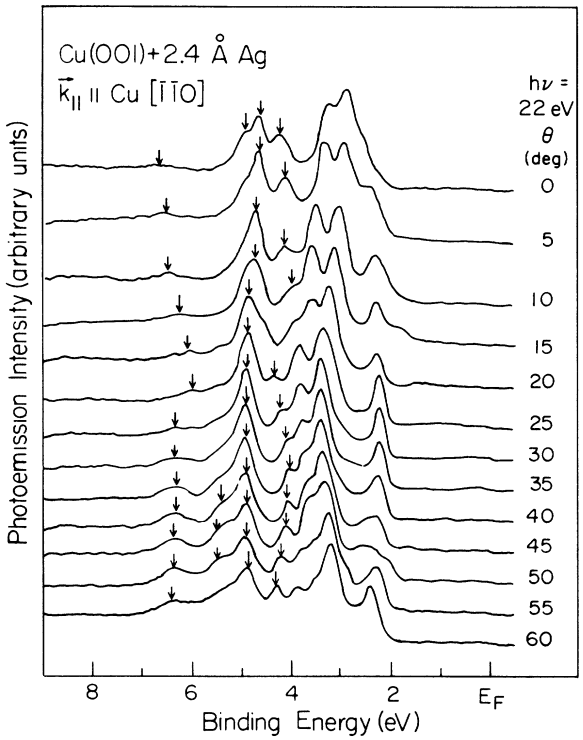

FIG. 6. Same as Fig. 3 except that the sample is 2.4 Å (1 ML) of Ag on Cu(001) forming a $c(10\times2)$. The scan direction is indicated.

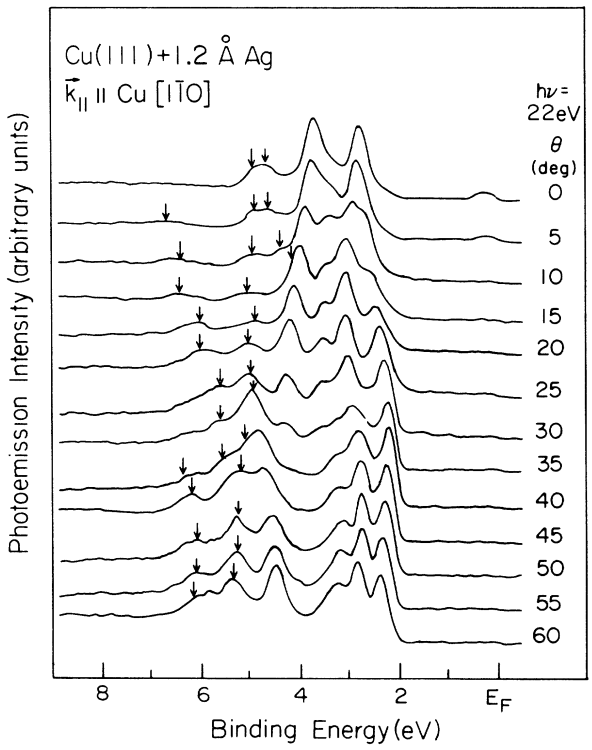

FIG. 5. Same as Fig. 3 except for a different scan direction as indicated.

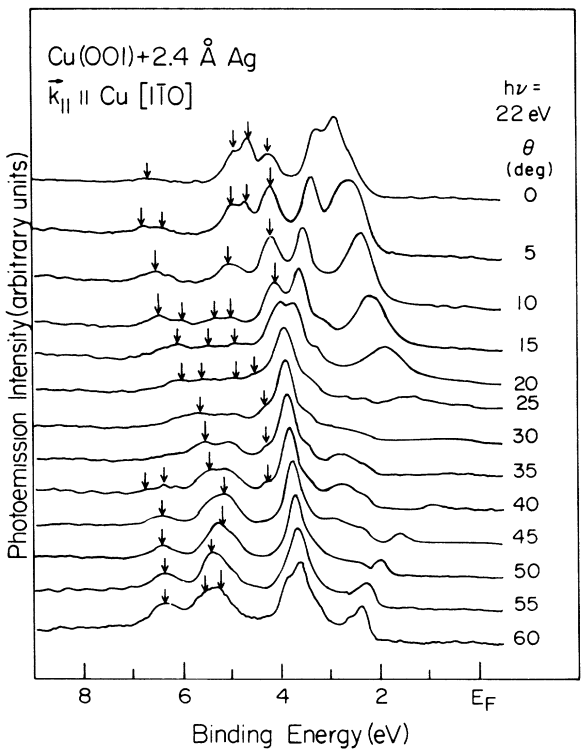

FIG. 7. Same as Fig. 6 except for a different scan direction as indicated.

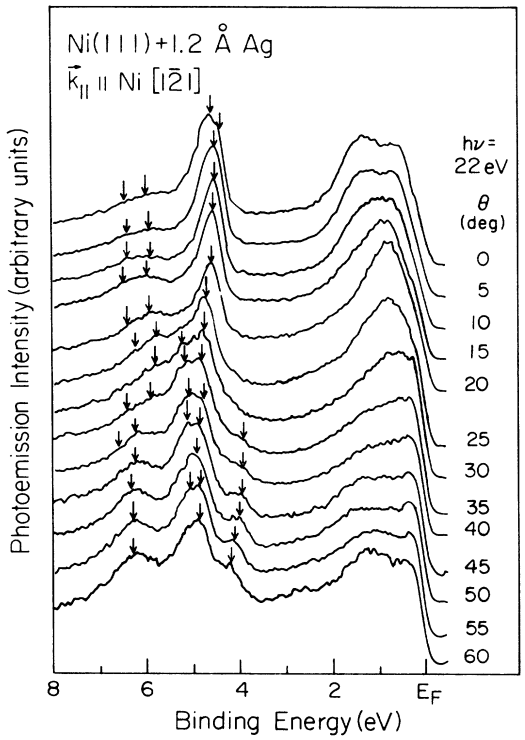

FIG. 8. Same as Fig. 3 except that the sample is 1.2 Å ($\frac{1}{2}$ ML) of Ag on Ni(111).

16. Because the degree of attenuation of the photoelectron current depends on the photoelectron kinetic energy and is not known precisely, the two spectra used to generate each of these difference spectra were normalized (independent of energy) by inspection before subtraction. As a result, some of the substrate features still appear in these difference spectra, although at a greatly reduced intensity. In a few locations there are "dips" from excessive substrate signal subtraction. Even with the difference spectra, the origin of some of the spectral features is not clear. For example, the source of the normal emission feature with a binding energy of 6.09 eV is not as easily determined, since both Ag and Au have bands located close to the position of the observed feature. In order to resolve this problem, the spectra for Ag coverages of 0 and $\frac{3}{4}$ ML were compared with spectra taken at 2 ML Ag coverage (not shown) in both a normal and off-normal geometry. As the thickness of the Ag overlayer on the Au substrate is increased, the feature at 6.09 eV binding energy remains quite intense and shifts slightly in energy when observed in normal emission. In off-normal scans, the separation between the Au feature and the feature at $\frac{3}{4}$ ML Ag coverage becomes as large as 0.2 eV. Therefore, this feature is at least partially derived from the Ag overlayer.

Compared with the other systems studied here, the spectra for Ag on Si(111) were very broad. Furthermore, changing the analyzer collection angles did not cause the

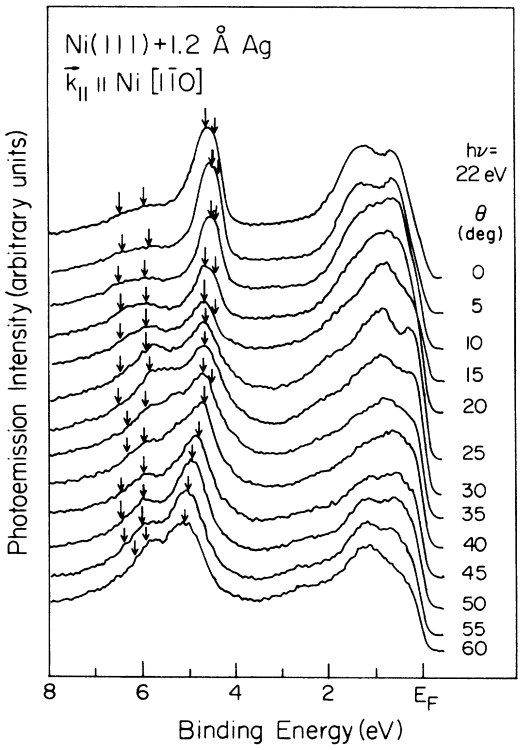

FIG. 9. Same as Fig. 8 except for a different scan direction as indicated.

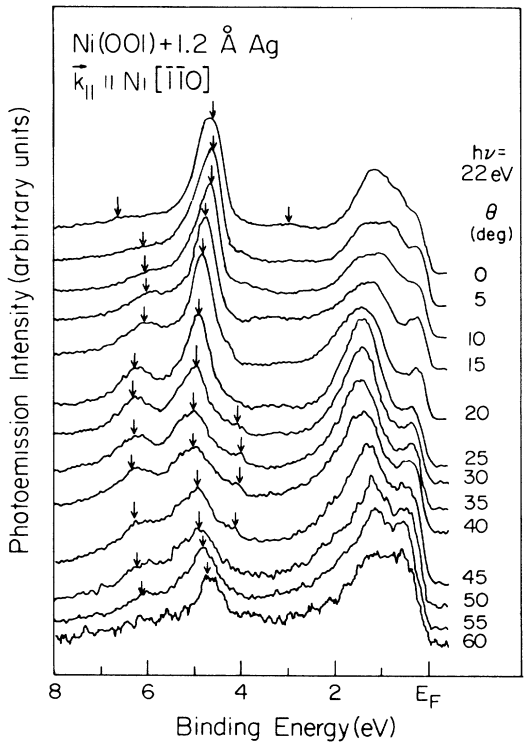

FIG. 10. Same as Fig. 3 except that the sample is 1.2 Å ($\frac{1}{2}$ ML) of Ag on Ni(001). The scan direction is indicated.

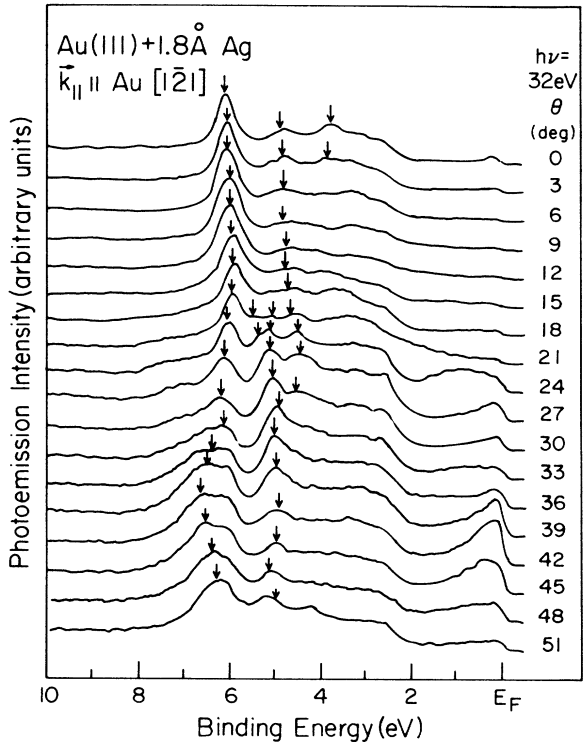

FIG. 11. Angle-resolved photoemission spectra from 1.8 Å ($\frac{3}{4}$ ML) of Ag on Au(111) taken with a photon energy of 32 eV. The direction of $\mathbf{k}_{\parallel}$ in the scan and the polar emission angles θ are indicated. Features which are due to the presence of the Ag overlayer are marked with arrows. The binding energies are referred to the Fermi level at E_F.

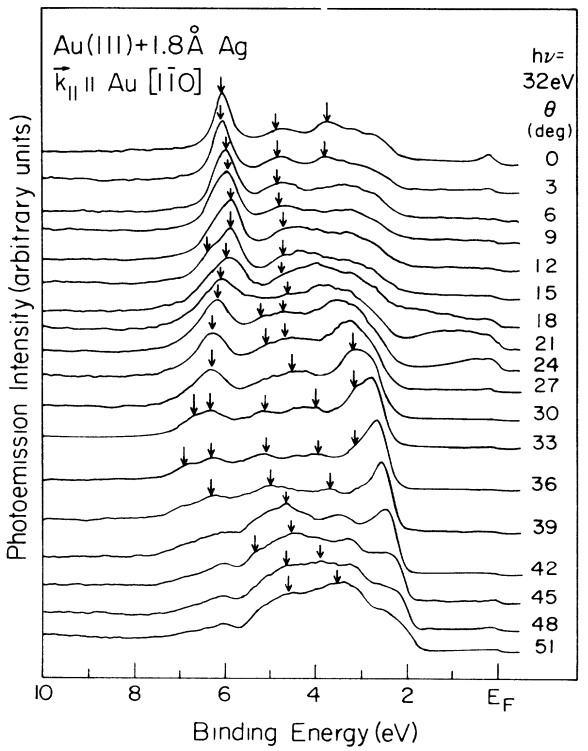

FIG. 12. Same as Fig. 11 except for a different scan direction as indicated.

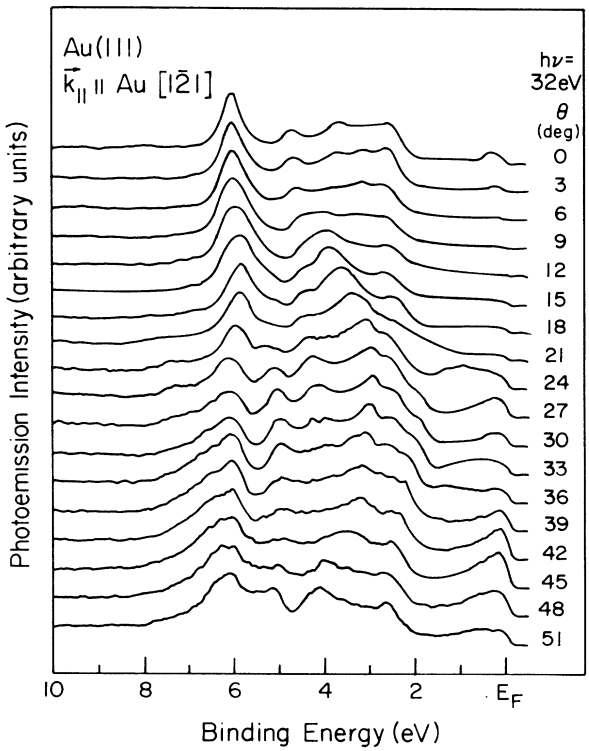

FIG. 13. Same as Fig. 11 except without the Ag overlayer.

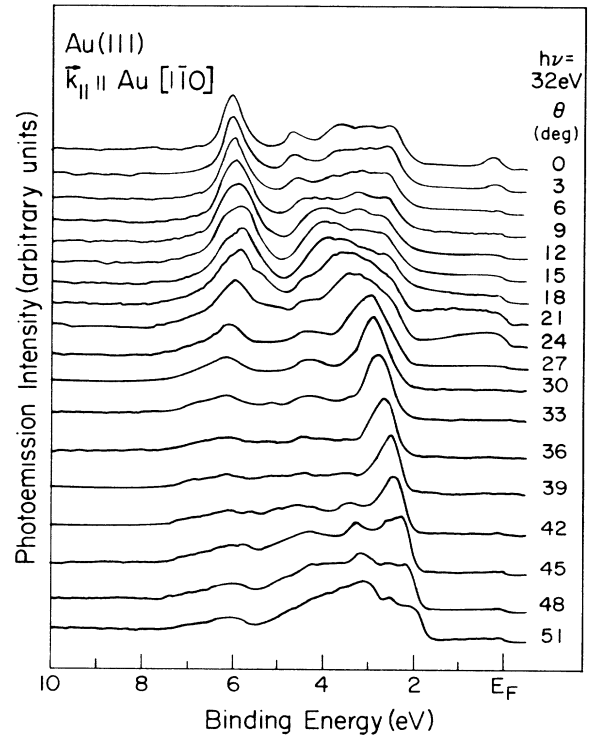

FIG. 14. Same as Fig. 12 except without the Ag overlayer.

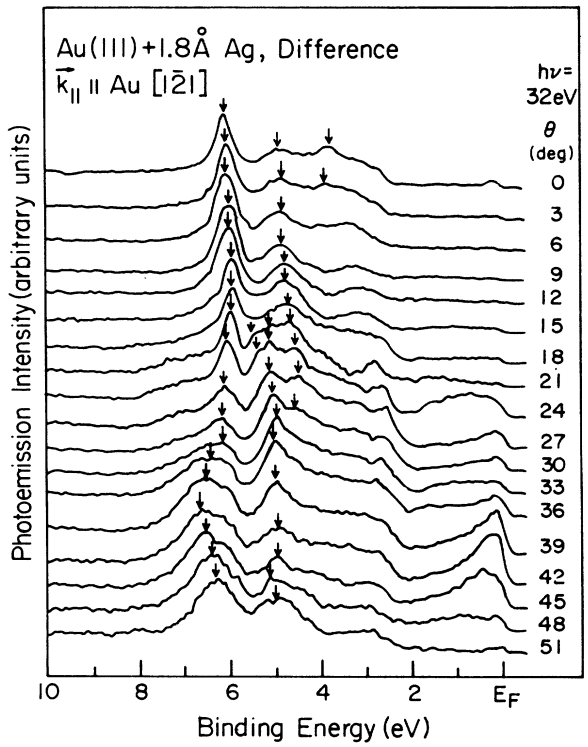

FIG. 15. Difference spectra for the Ag-Au(111) system obtained by subtracting the spectra shown in Fig. 13 (for the bare Au substrate) from the corresponding spectra shown in Fig. 11 (for Au covered with Ag). The scan direction is indicated.

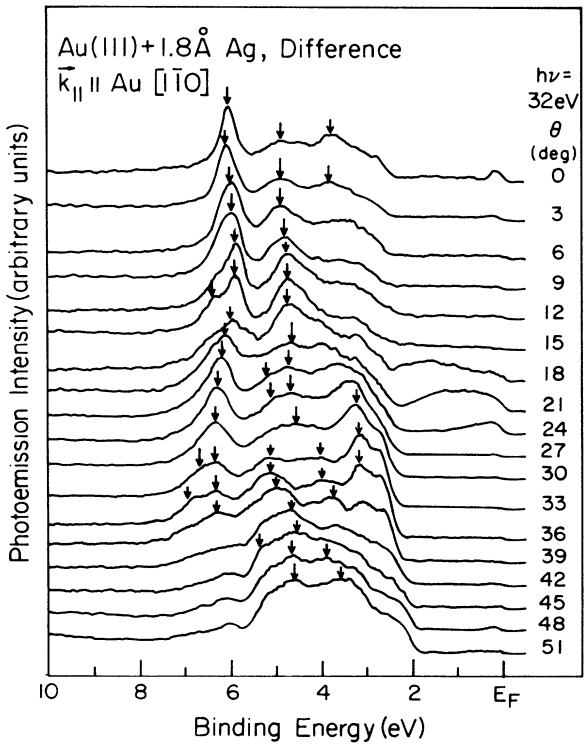

FIG. 16. Difference spectra for the Ag-Au(111) system obtained by subtracting the spectra shown in Fig. 14 (for the bare Au substrate) from the corresponding spectra shown in Fig. 12 (for Au covered with Ag). The scan direction is indicated.

line shape to change appreciably. These observations suggest that the Ag overlayer is not as well ordered as the other systems, and the photoemission spectra, even though angle resolved, reflect roughly the density of states. There is no point in showing all of the spectra here, as they are all very similar. Instead, we show in Fig. 17 normal emission spectra for all six Ag-covered substrates, taken with a 22-eV photon energy. The peaks which are Ag derived are marked with vertical bars. Except for Ag on Si(111), the spectra show overall similarities as suggested by the dashed lines. For Ag on Au(111), the peak at 6.09 eV binding energy is marked with a question mark to indicate that this peak has unresolved partial contributions from both the Ag overlayer and the Au substrate as discussed above.

C. Two-dimensional band dispersions

Following standard procedures and assuming direct transitions without umklapp, the two-dimensional band dispersions for the Ag(111) overlayer systems, except Ag-Si(111) for reasons discussed above, have been determined from the data presented here. The results are displayed in Figs. 18–27 for each of the two scan direc-

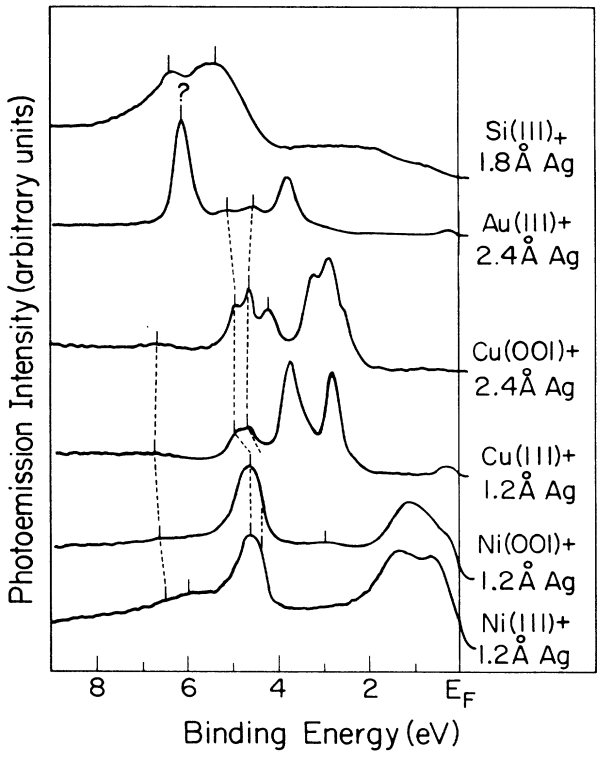

FIG. 17. Normal emission spectra from all six Ag overlayer systems taken with a photon energy of 22 eV. The substrate face and overlayer coverage are indicated. Features which are due to the presence of the Ag overlayer are marked with vertical bars. The binding energies are referred to the Fermi level at E_F. The peak marked by a question mark has only partial contribution from the Ag.

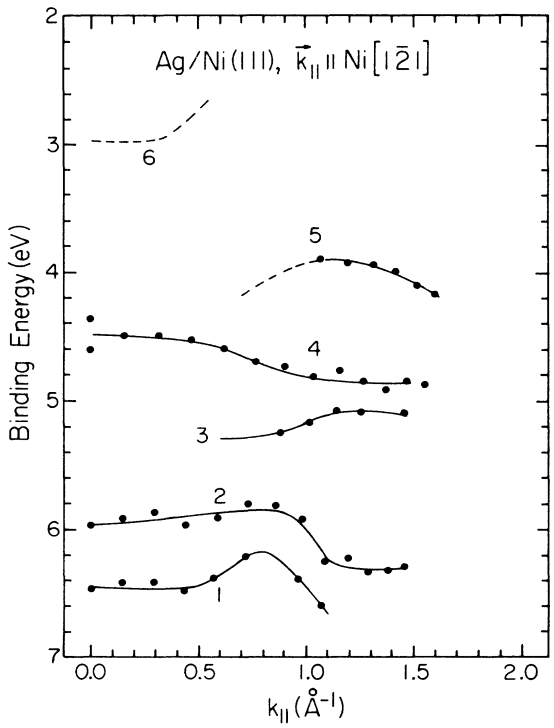

FIG. 18. Two-dimensional band dispersions for Ag on Ni(111). The direction of scan is indicated. The energy zero is the Fermi level. The smooth solid and dashed curves are "reference" dispersion curves discussed in the text.

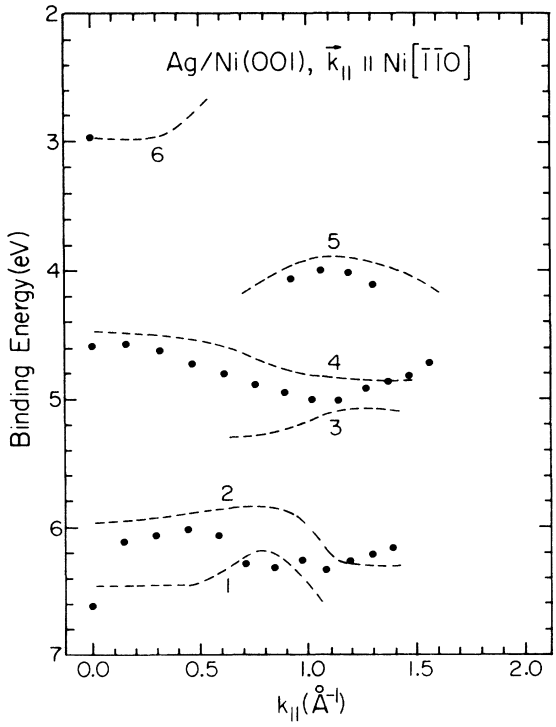

FIG. 20. Same as Fig. 18 except for Ag on Ni(001). The direction of scan is indicated.

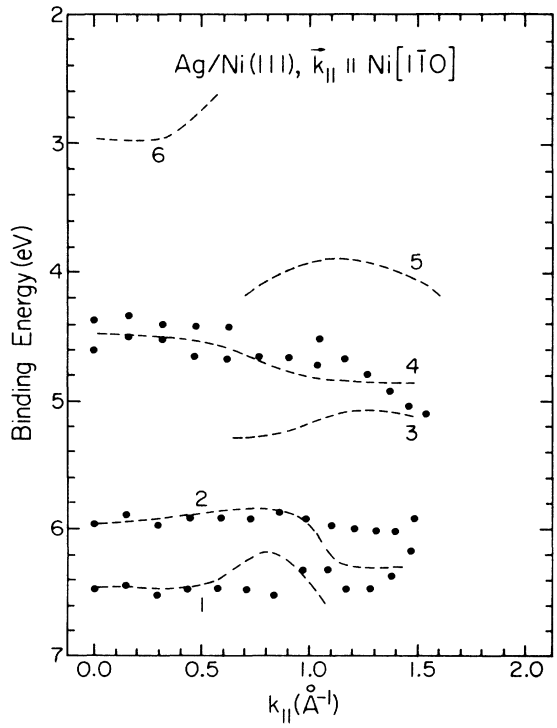

FIG. 19. Same as Fig. 18 except for a different scan direction as indicated.

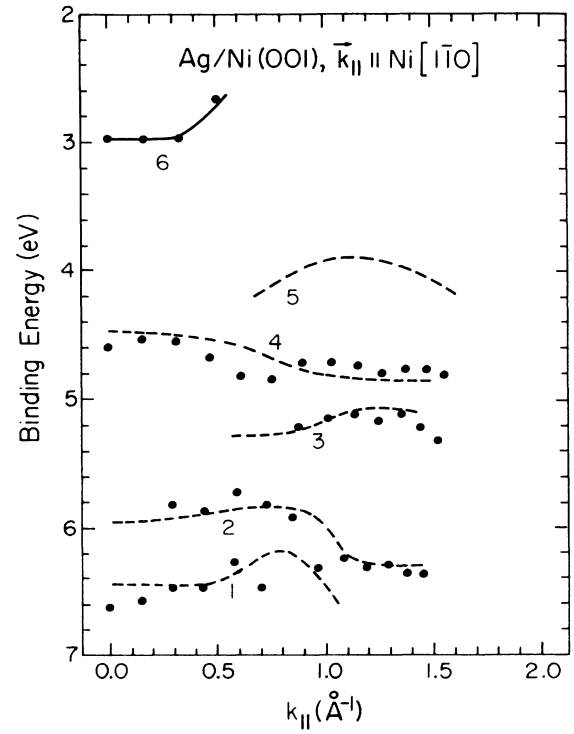

FIG. 21. Same as Fig. 20 except for a different direction of scan.

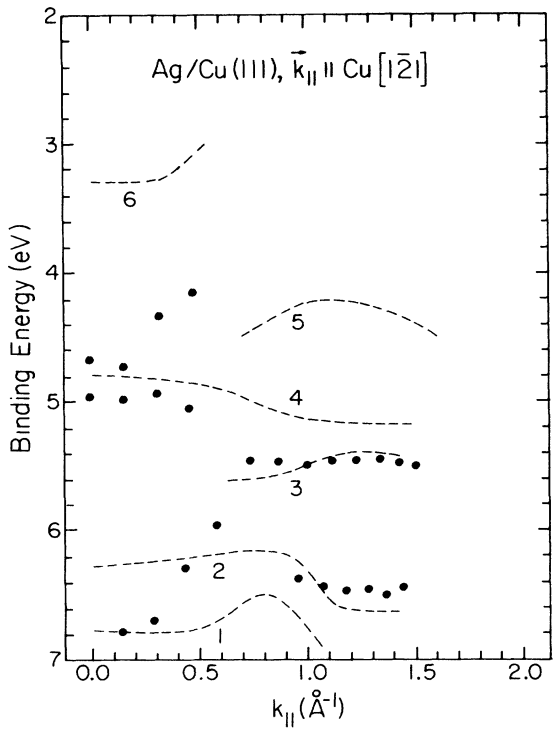

FIG. 22. Same as Fig. 18 except for Ag on Cu(111).

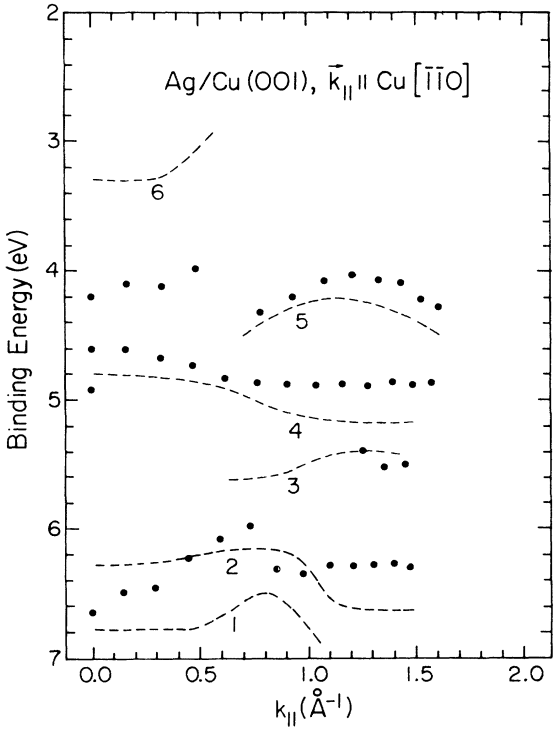

FIG. 24. Same as Fig. 18 except for Ag on Cu(001). The direction of scan is indicated.

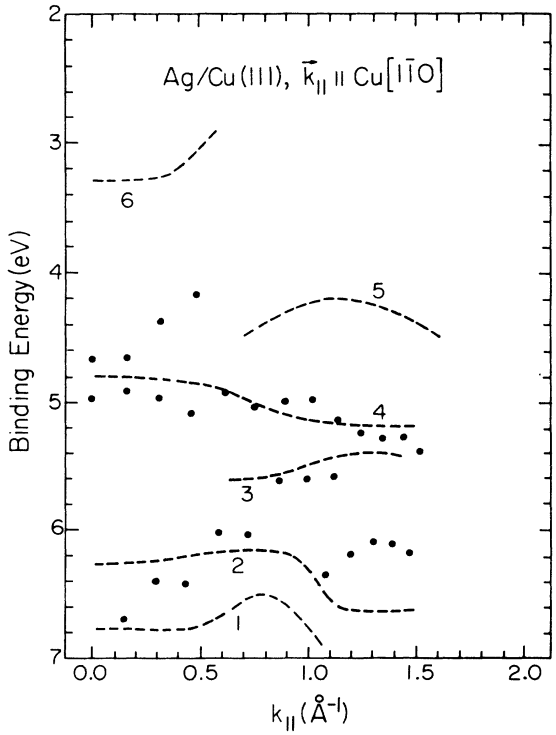

FIG. 23. Same as Fig. 22 except for a different direction of scan as indicated.

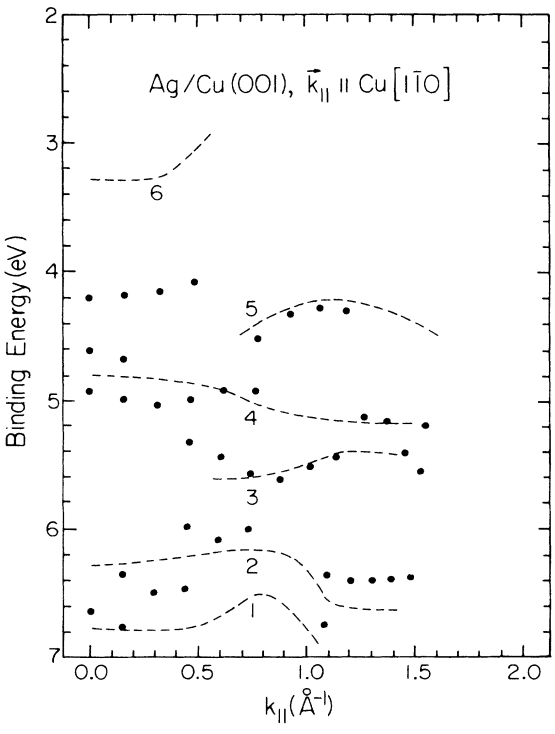

FIG. 25. Same as Fig. 24 except for a different direction of scan as indicated.

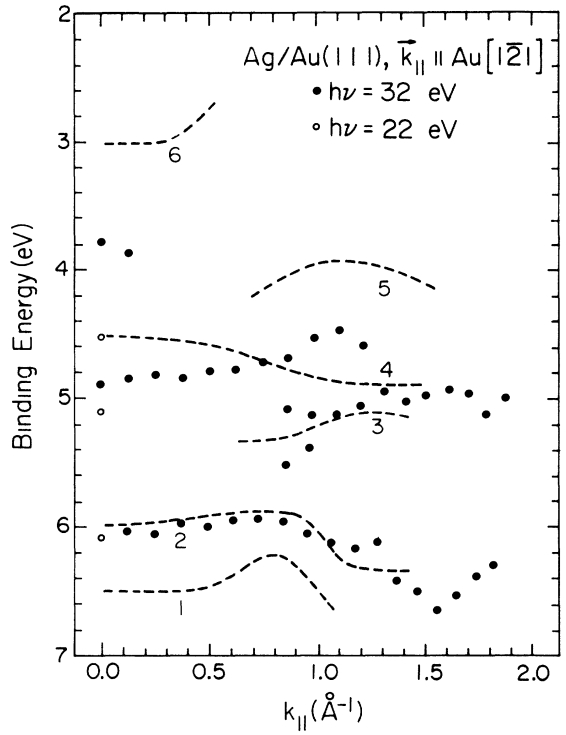

FIG. 26. same as Fig. 18 except for Ag on Au(111).

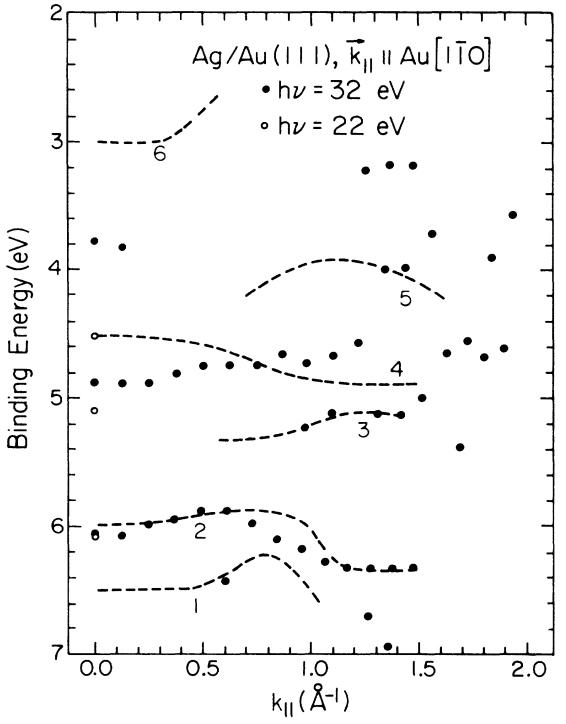

FIG. 27. Same as Fig. 26 except for a different direction of scan as indicated.

tions in the five systems. The data points (circles) can be uncertain by ±0.1 to 0.2 eV for peaks not well resolved; there is also some uncertainty in the calculated value of $k_{\parallel}$ as a result of the finite acceptance angle. Unresolved peaks are indicated only by the average peak positions. The system of $c(10\times2)$ Ag on Cu(001) has also been investigated in detail by Tobin and collaborators under different experimental conditions;[4–6] our results are in good agreement with theirs in regions where the two sets of data overlap.

IV. DISCUSSIONS

It is difficult to compare all of the band dispersions shown in Figs. 18–27 simultaneously. However, the results for most of the systems show overall similarities. Therefore, a set of fixed "reference" dispersion curves are generated mainly based on the Ni and Cu substrate data. The assumption is made here that the Ag overlayer states are, to the first order, independent of the substrate; therefore, the various states in the different systems can be related. The evidence leading to this assumption includes the similarities in the relative photoemission cross sections as well as the similarities in the band dispersions. The reference curves are shown as either solid or dashed curves in the figures. Solid curves in the figures are used to indicate that a curve has been derived from nearby points in that particular figure, whereas dashed curves are derived from other figures or are visually determined "average" curves. An overall energy shift has been applied to the set of reference curves for each substrate material where necessary to produce the best visual agreement with the data. The shift can be justified by noting that there is generally a shift in the average electrostatic potential within a supported film for different substrates. The value of the shift cannot be predicted theoretically, but its order of magnitude can be estimated.[2] We have found that for a given substrate material (Ni or Cu) there is no need to introduce a relative shift between the data for the (100) and (111) substrate faces. The shifts used here are 0.32 and 0.03 eV toward higher binding energies for the Cu and Au substrates, respectively, relative to the Ni substrates. Note that there are six reference curves, labeled 1–6. Because each Ag atom has one *sp* and five *d* electrons, six bands are expected if spin-orbit splitting (and/or crystal-field splitting) is ignored. The data clearly indicate that the splitting is present; for example, the data for Cu(001), Cu(111), and Ni(111) show a splitting of about 0.2–0.4 eV for band 4 at the surface zone center.[4–6] The corresponding splitting for the Ni(001) data was not observed, probably because it is too small.

A. Comparing the band dispersions along $\bar{\Gamma}\bar{K}$ and $\bar{\Gamma}\bar{M}$ for a given substrate

For Ag monolayers on Ni(111), Cu(111), and Au(111), the two scans for $\mathbf{k}_{\parallel}$ along the $\bar{\Gamma}\bar{M}$ and $\bar{\Gamma}\bar{K}$ directions yield very similar band dispersions, especially near the zone center (see Figs. 18, 19, 21, 22, 26, and 27). At the zone center, the two sets of dispersion curves should meet. Near the zone center, the dispersion relations

$E(\mathbf{k}_\parallel)$ can be expanded in powers of the components of $\mathbf{k}_\parallel$. The symmetry of the system is sufficiently high so that if the expansion is kept only to the second order (the first-order terms vanish), the constant energy surfaces are concentric circles about the zone center. Thus, the curvatures of the dispersion curves along the two different directions should be the same near the zone center. This explains the similarities between the dispersion curves for the two directions. For larger values of $k_\parallel$, the dispersions will become different, as observed experimentally. This symmetry argument is independent of the electronic properties of the substrate material.

For the Ni(001) and Cu(001) substrates, the two scans along different directions yield band dispersions along the $\bar{\Gamma}\bar{M}$ and $\bar{\Gamma}\bar{K}$ directions simultaneously due to the presence of two orthogonal domains. Therefore, the band dispersions shown in Figs. 20, 21, 24, and 25 represent a mixture along these two directions. Based on the argument given above, we expect that near the zone center the two sets of dispersion curves are nearly coincident and cannot be separated. For larger values of $k_\parallel$, the two sets will generally have different shapes. However, the photoemission cross sections for the different states may be such that only some of these states are observed experimentally. In addition, these different states may be quite close to yield unresolved peaks in the photoemission spectra. These possibilities can explain the fact that only a small number of peaks are observed in the spectra.

B. Comparing the band dispersions for different faces of a given substrate material

With the aid of the reference curves, one can see that the band dispersions for Ag-Ni(111) and Ag-Ni(001), shown in Figs. 18–21, are remarkably similar, bearing in mind that the (001) results are a mixture along the two symmetry directions. An association of the data points for the two faces can be easily established. In fact, most of the corresponding data points fall within the joint uncertainties. In addition, the relative photoemission intensities for the different states are very similar for the two faces under similar experimental conditions (see Figs. 8–10).

The same conclusion is reached for a comparison of the band dispersions for the Cu(111) and Cu(001) substrates (see Figs. 22–25). The relative photoemission intensities for the different states (see Figs. 3 and 5–7) are also fairly similar except for one peak (see below).

C. Comparing the band dispersions for different substrate materials

By comparing the band dispersions shown in Figs. 18–25 and the corresponding photoemission spectra in Figs. 3 and 5–10, one can see that the experimental band structures for Ag on the Ni and Cu substrates are very similar. The only pronounced difference is the fairly intense spectral feature for the Cu(001) substrate at a binding energy of 4.0–4.2 eV and for $\mathbf{k}_\parallel$ near the zone center; this feature is not observed in the corresponding Ni data. A similar peak is also observed in the Cu(111) spectra; however, it is much weaker and is observed only within a much smaller range of $\mathbf{k}_\parallel$. This peak has been previously assigned as possibly an umklapp peak because it evolves into an indirect transition peak when the Ag overlayer thickness is increased. However, the interpretation is still being debated.[4–6]

The results for Ag-Au(111) shown in Figs. 26 and 27 are more dissimilar when compared with the other systems. The most intense photoemission features for $\mathbf{k}_\parallel$ near the zone center are derived from band 4. Note that the Ni and Cu data show a nearly identical negative curvature for this band near the zone center, while the Au data show a positive curvature instead. Furthermore, there are many data points at larger $k_\parallel$ values for the Ag-Au(111) system which clearly cannot be described by the reference dispersion curves.

D. General trend

Based on the above comparisons, we can arrive at several general comments about the behavior of these systems. These comments will need confirmation when rigorous theoretical calculations become available. They also need to be checked when experimental results from other monolayer systems become available.

The observation that the band structures for Ag on Ni(001), Ni(111), Cu(001), and Cu(111) are all very similar tends to suggest that the band dispersions are determined, to the first order, by the interactions within the Ag monolayer itself. Thus, the substrate atomic structure and electronic properties play a much less important role in determining the overlayer band dispersions. Note that Ni has partially filled d bands, while Cu has completely filled d bands. The difference, though, seems to cause just an overall shift in the electrostatic potential in the overlayer and hence an overall shift in the band dispersions.

The band dispersions are a result of the periodic potential within the lattice, as discussed in any standard solid-state textbook. For Ag on Ni(111), Ni(001), and Cu(111), the overlayer and the substrate are incommensurate. Thus the interaction between the overlayer and the substrate results in a term in the Hamiltonian for the electrons in the Ag overlayer, which is incommensurate with respect to the overlayer lattice. If this interaction term can be considered as a perturbation, it cannot introduce a coherent scattering of the electron wave functions within the Brillouin zone, and hence the shape of the dispersion curves cannot be modified to the first order. Within a mean-field approximation, each Bloch state $\psi(\mathbf{k}_\parallel)$ within the overlayer is equally coupled to all other Bloch states with arbitrary $\mathbf{k}_\parallel$; thus, the net effect of the perturbation is simply an overall shift of the energy, independent of $\mathbf{k}_\parallel$. The effect of the incommensurate perturbation is just like that of a random perturbation. Presumably, the perturbation is sufficiently small that the wave functions in the Ag overlayer can still be described by Bloch states. Note that this argument is valid only if the wave functions in the overlayer are decoupled from those in the substrate; namely, the overlayer wave functions remain localized within the overlayer. This is approximately true for Ag

on Ni and Cu, as the $E(\mathbf{k})$ dispersion curves show large mismatches.

For Ag on Cu(001), a $c(10\times2)$ commensurate structure is formed. Yet the period of commensuration is rather large; thus the substrate-overlayer interaction term will have spatial Fourier components characterized by basis vectors much smaller than the size of the original (1×1) Brillouin zone. The limit of a very large period of commensuration is equivalent to incommensuration. In the present case, the perturbation couples a given Bloch state to many (although finite) other values of $\mathbf{k}_{\parallel}$ within the Brillouin zone, resulting in a smearing of the effect. Thus, the results for Ag on Cu(001) are still fairly similar to the other three cases discussed above. It has been pointed out that the most pronounced difference for this system is the fairly intense spectral feature at a binding energy of 4.2 eV in the normal emission spectrum (Fig. 17), which is not observed in the other systems. The earlier assignment that this is an umklapp feature is consistent with the present interpretation,[2,4–6] since the commensurate perturbation is more likely to give rise to umklapp transitions.

For Ag on Au(111), the epitaxial relationship is an almost perfect, lattice-matched (1×1). Based on the above argument, one expects that the substrate potential will have a much larger effect on the shape of the overlayer band dispersions. Indeed, the Ag band dispersions appear to be quite different from those of the other systems. Furthermore, the Ag and Au states show substantial overlap within the energy range of interest; thus, there is a possibility that some of the overlayer-derived states may no longer be localized within the overlayer. Some of the wave functions in Ag and Au may be joined together across the boundary to form, for example, surface resonances.[10,29] This effect can cause significant modifications to the overlayer electronic properties.

The results for Ag on Si(111) would be similar to those for Ag-Ni and Ag-Cu, as the overlayer and the substrate are incommensurate. But in this case, the substrate is quite "rough" on an atomic scale, causing the overlayer ordering to be much worse than the other systems. The Si(111)-(7×7) surface structure is known to have adatoms, stacking faults, and deep holes.[40] The large distortion in the overlayer structure due to substrate roughness can lead to a large perturbation in the crystal potential, which can in turn cause severe incoherent scattering of all the Bloch states. It is conceivable that the structural imperfection renders the $\mathbf{k}_{\parallel}$ values very much smeared, so that only the density of states is probed with angle-resolved photoemission. Furthermore, if the perturbation is sufficiently strong, the electronic states within the Ag overlayer may become localized and a Bloch state description may cease to be valid. Disorder-induced electronic localization is a well-documented phenomenon, and is known to be important in glassy materials.

V. CONCLUSIONS

This study has examined the growth and electronic properties of Ag(111) monolayers on six different substrates: Ni(111), Ni(001), Cu(111), Cu(001), Au(111), and Si(111)-(7×7). The two-dimensional band dispersions for the Ag valence states have been obtained via photoemission along high-symmetry directions for these systems except Ag-Si(111). The results provide a data base for making some general comments about the effects of the substrate on the overlayer electronic properties.

On the Cu(111), Ni(001), and Ni(111) substrates, where Ag(111) grows in an incommensurate fashion, the overlayer band structures are very similar despite the large differences in the electronic and atomic structures of the substrates. The $c(10\times2)$Ag-Cu(001) system, although commensurate, also shows fairly similar band structures, probably because of the large size of the reconstruction unit cell. An extra spectral feature can be attributed to umklapp transitions induced by the commensuration. In the case of Ag-Au(111), the overlayer grows in a lattice-matched fashion, and its band dispersions have a different appearance. These similarities and differences are explained in terms of the degree of commensuration of the substrate-overlayer interaction as a perturbation. The growth of Ag on Si(111)-(7×7) is not as well ordered as in the other systems. A severe broadening of the overlayer features is observed. Momentum broadening as well as random crystal potential variation within the overlayer are likely to be the cause. In light of these measurements, it will be useful to examine this problem with state-of-the-art calculations.

ACKNOWLEDGMENTS

This material is based upon work supported by the National Science Foundation under Contract No. DMR-8614234. Some of the personnel and equipment used for this research were also supported by grants from the National Science Foundation (Grant No. DMR-8352083), the IBM Thomas J. Watson Research Center (Yorktown Heights, NY), the E. I. du Pont de Nemours and Company (Wilmington, DE), the 3M Company (Saint Paul, MN), and the Hewlett Packard Laboratory (Palo Alto, CA). The Synchrotron Radiation Center of the University of Wisconsin–Madison is supported by the National Science Foundation under Contract No. DMR-8020164. We acknowledge the use of central facilities of the Materials Research Laboratory of the University of Illinois, which is supported by the U.S. Department of Energy, Division of Materials Sciences, under Contract No. DE-AC02-76ER01198, and the National Science Foundation under Contract No. DMR-8316981.

*Present address: IBM East Fishkill Facility, Hopewell Junction, NY 12533-0999.

†Present address: Microelectronics Materials Center, Polaroid, Cambridge, MA 02139.

‡Present address: Lawrence Livermore National Laboratory, Livermore, CA 94550.

[1] A. P. Shapiro, A. L. Wachs, T. C. Hsieh, T. Miller, P. John, and T.-C. Chiang, Phys. Rev. B **34**, 7425 (1986).

[2]A. P. Shapiro, A. L. Wachs, T. Miller, and T.-C. Chiang, Solid State Commun. **55**, 1101 (1985).
[3]K. Gurtler and K. Jacobi, Surf. Sci. **134**, 309 (1983).
[4]J. G. Tobin, S. W. Robey, L. E. Klebanoff, and D. A. Shirley, Phys. Rev. B **28**, 6169 (1983).
[5]J. G. Tobin, S. W. Robey, and D. A. Shirley, Phys. Rev. B **33**, 2270 (1986).
[6]J. G. Tobin, S. W. Robey, L. E. Klebanoff, and D. A. Shirley, Phys. Rev. B **35**, 9056 (1987).
[7]T. W. Capehardt *et al.*, J. Vac. Sci. Technol. A **1**, 1214 (1983).
[8]R. Miranda, F. Yndurain, D. Chandesris, J. Lecante, and Y. Petroff, Phys. Rev. B **25**, 527 (1982); Surf. Sci. **117**, 319 (1982).
[9]R. Miranda, D. Chandesris, and J. Lecante, Surf. Sci. **130**, 269 (1983).
[10]P. Steiner and S. Hufner, Solid State Commun. **37**, 279 (1981).
[11]M. El-Batanouny, D. R. Hamann, S. R. Chubb, and J. W. Davenport, Phys. Rev. B **27**, 2575 (1983); M. El-Batanouny, M. Strongin, and G. P. Williams, *ibid.* **27**, 4580 (1983).
[12]P. J. Feibelman and D. R. Hamann, Phys. Rev. B **28**, 3092 (1983).
[13]S. Ohnishi, M. Weinert, and A. J. Freeman, Phys. Rev. B **30**, 36 (1984).
[14]D.-S. Wang, A. J. Freeman, and H. Krakauer, Phys. Rev. B **26**, 1340 (1982).
[15]R. H. Victora and L. M. Falicov, Phys. Rev. B **29**, 5253 (1983).
[16]I. Abatti *et al.*, Phys. Rev. Lett. **40**, 469 (1978).
[17]B. R. Cooper, Phys. Rev. Lett. **30**, 1316 (1973).
[18]O. Jepsen, J. Madsen, and O. K. Anderson, Phys. Rev. B **18**, 605 (1978).
[19]G. S. Painter, Phys. Rev. B **17**, 3848 (1978).
[20]E. Wimmer, J. Phys. F **14**, 2613 (1984).
[21]F. J. Arlinghaus, J. G. Gay, and J. R. Smith, Phys. Rev. B **20**, 1332 (1979).
[22]G. S. Wang and A. J. Freeman, Phys. Rev. B **18**, 1714 (1978); **19**, 793 (1979); **21**, 4585 (1980).
[23]W. J. McG. Tegart, *The Electrolytic and Chemical Polishing of Metals* (Pergamon, London, 1956).
[24]R. Courths and S. Hufner, Phys. Rep. **112**, 53 (1984), and references therein.
[25]R. Courths *et al.*, J. Phys. F **14**, 1559 (1984).
[26]P. Heimann, H. Neddermeyer, and H. F. Roloff, J. Phys. C **10**, L17 (1977).
[27]F. J. Himpsel and D. E. Eastman, Phys. Rev. Lett. **41**, 507 (1978).
[28]A. L. Wachs, T. Miller, T. C. Hsieh, A. P. Shapiro, and T.-C. Chiang, Phys. Rev. B **32**, 2326 (1985).
[29]T. C. Hsieh and T.-C. Chiang, Surf. Sci. **166**, 554 (1986).
[30]T. C. Hsieh, T. Miller, and T.-C. Chiang, Phys. Rev. Lett. **55**, 2483 (1985).
[31]T. C. Hsieh, T. Miller, and T.-C. Chiang, Phys. Rev. B **33**, 2865 (1986).
[32]A. P. Shapiro, A. L. Wachs, and T.-C. Chiang, Solid State Commun. **58**, 121 (1986).
[33]A. P. Shapiro, T. Miller, and T.-C. Chiang, Phys. Rev. B **37**, 3996 (1988).
[34]G. LeLay, M. Manneville, and R. Kern, Surf. Sci. **72**, 405 (1978).
[35]R. J. Culbertson, L. C. Feldman, P. J. Silverman, and H. Boehm, Phys. Rev. Lett. **47**, 657 (1981).
[36]A. L. Wachs, A. P. Shapiro, T. C. Hsieh, and T.-C. Chiang, Phys. Rev. B **33**, 1460 (1986).
[37]A. L. Wachs, T. Miller, and T.-C. Chiang, Phys. Rev. B **29**, 2286 (1984).
[38]L. G. Feinstein, E. Blanc, and D. Dufayard, Surf. Sci. **19**, 269 (1970).
[39]D. C. Jackson, T. E. Gallon, and A. Chambers Surf. Sci. **36**, 381 (1973).
[40]K. Takayanagi, Y. Tanishiro, M. Takahashi, and S. Takahashi, J. Vac. Sci. Technol. A **3**, 1502 (1985).